1-1-2004

# Three-wave solitons and continuous waves in media with competing quadratic and cubic nonlinearities

Min Chen

D. J. Kaup
*University of Central Florida*

Boris A. Malomed

# Three-wave solitons and continuous waves in media with competing quadratic and cubic nonlinearities

Min Chen,[1] D. J. Kaup,[2] and Boris A. Malomed[3]

[1]*Department of Mathematics, Purdue University, West Lafayette, Indiana 47907, USA*
[2]*Department of Mathematics, and the Institute for Simulation & Training, University of Central Florida, P.O. Box 161364, Orlando, Florida 32816-1364, USA*
[3]*Department of Interdisciplinary Studies, Faculty of Engineering, Tel Aviv University, Tel Aviv 69978, Israel*

We formulate a general model of three-wave optical interactions (in the spatial domain), which combines quadratic ($\chi^{(2)}$) and cubic ($\chi^{(3)}$) nonlinearities, the latter including four-wave mixing. The model can be realized in $\chi^{(2)}$ materials where an effective $\chi^{(3)}$ nonlinearity is engineered by means of the quasi-phase-matching technique. Both self-focusing and self-defocusing $\chi^{(3)}$ nonlinearities are considered. The birefringence of the two fundamental-frequency (FF) waves is taken into regard. Several types of solitons in this system are found, by means of the variational approximation and numerical methods. These are exact single-component solitons and generic three-wave (3W) ones, which are classified by relative signs of their components. Stability of the solitons is investigated by means of the Vakhitov-Kolokolov (VK) criterion, and then tested by direct simulations. One type of the single-component FF solitons (the "fast" one, in terms of the known two-component birefringent $\chi^{(3)}$ model) is, chiefly, unstable, as in that model, but nevertheless a *stability interval* is found for it, which provides for the first example of stable fast solitons. The other FF soliton (the "slow" one, in terms of the same $\chi^{(3)}$ model, where it is always stable) has its stability and instability regions. A single-component soliton in the second harmonic (SH) is found too; it also has its *stability region*, contrary to the common belief that such a soliton must always be unstable due to the parametric interaction. The 3W solitons are stable indeed if this is predicted by the VK condition, in the case when all the three components are positive. Following variation of the $\chi^{(2)}$ mismatch parameter, the 3W soliton bifurcates from the SH one, and at another point it bifurcates back into the slow-FF single-component soliton; conjectured normal forms of the respective bifurcations are given. 3W solitons with different signs of their components may be unstable *contrary* to the VK criterion, which is explained by consideration of the $\chi^{(2)}$ term in the system's Hamiltonian. In direct simulations, unstable solitons evolve into stable breathers. A different instability takes place in the case of the self-defocusing $\chi^{(3)}$ nonlinearity, when all the solitons blow up into a turbulent state. Parallel to the solitons, continuous-wave solutions are studied too. In terms of the existence and stability, they resemble solitons of similar types.

## I. INTRODUCTION

Solitons in optical media with the quadratic [$\chi^{(2)}$] nonlinearity, alias second-harmonic-generating (SHG) systems, is a subject that has been studied in detail theoretically and experimentally, see reviews [1] and [2]. An important case is the so-called type-II $\chi^{(2)}$ interaction, when the material birefringence is employed to phase-match two orthogonal linearly polarized components of the fundamental-frequency (FF) wave to a single second-harmonic (SH) component. In fact, this mechanism, which gives rise to stable three-wave (3W) solitary waves, was used in the first experimental observation of spatial $\chi^{(2)}$ solitons [3]. Basic properties of the 3W solitons were investigated in detail some time ago (see the above-mentioned reviews). Other effects that essentially affect dynamics of solitons, such as combination of linear mixing between the two FF polarizations and group-velocity birefringence, were considered more recently [4].

On the other hand, the $\chi^{(2)}$ interaction may compete with the less specific cubic [$\chi^{(3)}$, alias Kerr] nonlinearity. In two-wave (type-I) settings, the competition between the $\chi^{(2)}$ and $\chi^{(3)}$ nonlinearities was another subject of detailed studies (re-

sults can also be found in the reviews [1,2]). In uniform media admitting the phase-matched $\chi^{(2)}$ interaction, the natural Kerr nonlinearity is usually much weaker than its quadratic counterpart; nevertheless, in Ref. [5] it was demonstrated, in a direct experiment, that $\chi^{(2)}$ and $\chi^{(3)}$ nonlinearities can be made comparable in an optical crystal (actually, it was KTP) by properly adjusting the beam's Poynting vector relative to the crystallographic axes. Another possibility is to create a strong artificial $\chi^{(3)}$ nonlinearity of either sign (self-focusing or self-defocusing), which can be induced, in a basically $\chi^{(2)}$ medium, by means of the well-known QPM (quasi-phase-matching) technique, i.e., a periodic structure (grating) composed of alternating domains with opposite signs of the $\chi^{(2)}$ coefficient. This technique was first predicted as a means to create solitons supported by competing $\chi^{(2)}:\chi^{(3)}$ nonlinearities in Ref. [6]; later, an implementation in an optical crystal, employing sinusoidal modulation of the medium, was proposed in Ref. [7] (see also a review [8]). A still stronger $\chi^{(3)}$ interaction can be induced in two-period QPM gratings [9].

It should be stressed that the artificial $\chi^{(3)}$ nonlinearity induced via the QPM technique manifests a wider variety of

properties than its classical Kerr counterpart; in particular, the artificial nonlinearity may feature an arbitrary asymmetry between the FF and SH waves [for instance, with no $\chi^{(3)}$ self-phase modulation at the SH [6,7]; see also below]. Experimentally, an effective $\chi^{(3)}$ nonlinearity engineered on the basis of the fundamental SHG process in a QPM structure was first demonstrated in Ref. [10].

On the other hand, interplay of the Kerr nonlinearity and birefringence (in the absence of SHG interactions) is a well-investigated topic [11]. In particular, a known result is that, if the four-wave mixing (FWM) involving two linear polarizations is taken into regard, the soliton with the so-called *slow* polarization is stable, while the one with the orthogonal *fast* polarization is unstable [12] (exact definitions of the slow and fast, which refer to the birefringence, are given below).

A natural problem, that we will formulate and investigate in this work, is to search for soliton solutions, and analysis of their stability, in the 3W system which combines two orthogonally polarized FF components and a single SH one, taking the birefringence and both $\chi^{(2)}$ and $\chi^{(3)}$ nonlinearities into regard. Besides the solitons, we will also consider, in an analytical form, a similar but simpler problem for continuous-wave (CW) fields (in that case, the stability will be considered only against CW perturbations, while the modulational instability is not dealt with here).

In this 3W model, exact solutions can be found for single-component solitons, with only slow or fast FF component present. These solutions are obvious, as they nullify the $\chi^{(2)}$ terms and are identical to those found in the early work [12]. The first issue is stability of the slow and fast solitons, as it is not obvious that it must be exactly the same as in the model without the $\chi^{(2)}$ terms and SH component. We will conclude that, similar to the case considered in Ref. [12], the single-component fast solitons are unstable in most cases; nevertheless, an essentially novel result is that they may be *stable* in some parametric region. As for their slow counterparts, they may be both stable and unstable, on the contrary to the birefringent two-wave $\chi^{(3)}$ system, where they are always stable [12]. Besides that, an exact single-wave soliton containing only the SH component will be found too, being supported solely by the $\chi^{(3)}$ nonlinearity; quite unexpectedly, the latter soliton may be stable in some parameter region (it was commonly believed that such solitons are always unstable against FF perturbations).

A completely new problem is to find general 3W solitons in this model and analyze their stability. The formulation of the model itself is a novel issue too, as it includes some FWM terms that, to the best of our knowledge, have never been considered before, at least in the context of the $\chi^{(2)}:\chi^{(3)}$ competition (a multicomponent model of another type, combining $\chi^{(2)}$ and $\chi^{(3)}$ interactions, was recently considered in Ref. [13]).

A serious difficulty in studying this system in a systematic manner is to determine whether one has found all possible soliton solutions for the parameters given. Numerically searching the entire parameter space is not a realistic approach in the present context. Another path is followed in this work: we start with a more tractable CW counterpart of the model, in which stationary solutions are to be found from algebraic equations, rather than from ODEs. The set of the

CW solutions suggests how many their soliton counterparts, and of which types, are to be expected in the same parameter region. Then, we construct approximate soliton solutions in a (semi) analytical form by means of the variational approximation (VA; see a general review of this technique in Ref. [14]; a description of specific applications of VA to $\chi^{(2)}$ models can be found in the review [1]). Predictions concerning the stability of the 3W solitons will be first drawn by means of the known Vakhitov-Kolokolov (VK) criterion, which was proposed 30 years ago [15], and has been successfully applied to many models since then (see reviews [1,2,14] and [16]).

Analytical results produced by VA for both the shape of the stationary solitons and (in combination with the VK criterion) for their stability will then be tested against numerical solutions. We will conclude that the VA based on a Gaussian *ansatz* (trial wave form), which assumes equal widths of all the three components of the solitons, yields quite accurate results: basically, it predicts all the numerically found solitons (the only branch of soliton solutions that the VA fails to identify is one which strongly violates the assumption about equal widths in all the three components). The general structure of the soliton solutions is quite similar to that of the CW states. The solitons are found for both the self-focusing (Kerr) and self-defocusing (anti-Kerr) $\chi^{(3)}$ nonlinearities [in the latter case, solitons are possible provided that the $\chi^{(2)}$ nonlinearity is present]; however, the solitons are always unstable in the anti-Kerr case.

A fundamental result is that the 3W soliton with three positive components (therefore, it is labeled as a *PPP* one) presents, as a matter of fact, a crossover between two single-component solitons, *viz.*, SH and slow-FF ones: with the increase of the $\chi^{(2)}$ mismatch parameter, a stable 3W soliton bifurcates from a stable SH one; later, it becomes unstable, and, finally, it bifurcates into a weakly stable slow-FF soliton. We propose "phenomenological" normal forms of the two bifurcations, deferring a consistent derivation to another work. The 3W soliton of the *PPP* type is stable indeed where this is predicted by the VK criterion; however, 3W solitons containing negative components may be unstable contrary to this criterion, which we explain by consideration of the $\chi^{(2)}$ term in the system's Hamiltonian.

The VA generates parts of the soliton families in the present model at values of the propagation constant (intrinsic frequency) which belong to the continuous spectrum of the system's linearized version. This circumstance means that, in general, the corresponding parts of the solution branches represent *delocalized solitons*, i.e., pulses with nonvanishing oscillating tails [17]. Actually, it is not unusual for the VA to pick up such solutions [17]. In systems which support delocalized solitons, it frequently happens that, with the variation of the propagation constant, the amplitude of the tail crosses zero (vanishes) at certain points. If this happens, one has an *embedded* soliton (ES), which is a fully localized object that coexists with linear radiation modes (ESs were reviewed in recent papers [18]); however, search for ESs in the present system is beyond the scope of this paper.

For unstable solitons, we monitor their instability-triggered evolution by means of direct simulations. We conclude that the instabilities do not tend to turn unstable soli-

tons into other stationary stable ones, but rather transform them into very persistent *breathers*, i.e., solitary pulses featuring periodic internal vibrations. However, the instability-development scenario is very different in the case of the self-defocusing $\chi^{(3)}$ nonlinearity, resulting in a violent "blow-up" of the soliton (transition into a strongly turbulent state).

In the experiment, creation of stable 3W solitons should be possible in essentially the same range of physical parameters where two-wave optical solitons were earlier predicted in models with competing $\chi^{(2)}$ and $\chi^{(3)}$ nonlinearities (see reviews [1] and [2], and also Refs. [6]–[9] and the experimental work [10] for the most realistic case of the QPM-induced $\chi^{(2)}:\chi^{(3)}$ combined nonlinearity). In fact, the use of the birefringence, which usually helps to match the fundamental and second harmonics, may render the experimental creation of the soliton more feasible than in the usual two-wave system.

The rest of the paper is organized as follows. In Sec. II, the full 3W model is put forward; obvious solutions for the above-mentioned single-component solitons are also given in Sec. II. Section III reports investigation of CW solutions and their stability. Variational results for three-component solitons and predictions for their stability, based on the VK criterion, are given in Sec. IV. Results of direct numerical simulations (including formation of breathers from unstable solitons) are reported in Sec. V, which also presents conjectured normal forms describing bifurcations between the single-components and 3W solitons. The paper is concluded by Sec. VI.

## II. THE MODEL AND SIMPLE SOLUTIONS

A general 3W system combining the $\chi^{(2)}$ and $\chi^{(3)}$ nonlinearities and birefringence can be derived on the basis of the well-known model for the type-II SHG system [1,2], and the one for the copropagation of two orthogonal linear polarizations in the Kerr medium [12,11]. If the fields $u$ and $v$ are complex envelopes of the two components of the FF field, and $w$ is the single SH component, paraxial evolution equations, including the usual terms accounting for the type-II $\chi^{(2)}$ interaction and $\chi^{(3)}$ terms that take into regard the self-phase modulation (SPM), cross-phase modulation (XPM), and four-wave mixing (FWM), are

$$iu_z + \tfrac{1}{2}u_{xx} + v^*w + \gamma_1\left(\tfrac{1}{4}|u|^2 + \tfrac{1}{6}|v|^2 + 2|w|^2\right)u + \tfrac{1}{12}\gamma_1 v^2 u^*$$
$$+ \gamma_2|w|^2 v + bu = 0, \tag{1}$$

$$iv_z + \tfrac{1}{2}v_{xx} + u^*w + \gamma_1\left(\tfrac{1}{4}|v|^2 + \tfrac{1}{6}|u|^2 + 2|w|^2\right)v + \tfrac{1}{12}\gamma_1 u^2 v^*$$
$$+ \gamma_2|w|^2 u - bv = 0, \tag{2}$$

$$2iw_z + \tfrac{1}{2}w_{xx} + uv - qw + 2\gamma_1(2|w|^2 + |u|^2 + |v|^2)w$$
$$+ \gamma_2(uv^* + u^*v)w = 0, \tag{3}$$

where $b$ is a real birefringence coefficient, and $q$ is the phase-mismatch parameter that controls the SHG process. In these equations, the $\chi^{(2)}$ coefficient is normalized to be 1, while $\gamma_1$ and $\gamma_2$ are two $\chi^{(3)}$ coefficients. All these param-

eters are real, and they may be positive or negative, with a constraint that $\gamma_1$ and $\gamma_2$ must have the same sign. The cases $\gamma_{1,2}>0$ and $\gamma_{1,2}<0$ correspond, respectively, to the self-focusing (normal Kerr) and self-defocusing (anti-Kerr) $\chi^{(3)}$ nonlinearities.

If the cubic nonlinearity is directly induced by the electronic response of the dielectric medium, the two $\chi^{(3)}$ coefficients are not independent; it is easy to demonstrate that, in this case, they are related so that

$$\gamma_2 = \gamma_1/6. \tag{4}$$

If the cubic nonlinearity is induced by means of the above-mentioned QPM technique, the relation (4) does not necessarily hold, as the artificially induced $\chi^{(3)}$ terms may feature strong asymmetry between the FF and SH waves [6,7]. Nevertheless, for the definiteness' sake, we adopt the relation (4) hereafter (in fact, taking $\gamma_2$ different from $\gamma_1/6$ does not change any noteworthy aspect of the results).

It is obvious that the birefringence coefficient in Eqs. (1) and (2) can always be normalized so that $b \equiv 1$ (unless $b = 0$). Below, we will use this normalization in most cases. Thus, there remain two independent real parameters in the system, namely, the single free nonlinear coefficient $\gamma \equiv \gamma_1$ and the mismatch $q$.

Equations (1)–(3) are written for the paraxial evolution in the *spatial domain*, so that $z$ is the propagation distance, $x$ is the transverse coordinate in the corresponding planar waveguide, and the second derivatives account for transverse diffraction. A more general system, with independent coefficients in front of the second-derivative terms in different equations, may be introduced to describe the temporal-domain evolution, with $x$ replaced by the temporal variable. However, although temporal $\chi^{(2)}$ solitons have been observed in the experiment [19], spatial solitons in SHG systems are more feasible objects [1,2]. For this reason, we confine the model to its spatial-domain version.

Equations (1)–(3) conserve a dynamical invariant (power, alias the norm of the solution; in the temporal domain, it would be energy),

$$E = \int_{-\infty}^{+\infty} [|u(x)|^2 + |v(x)|^2 + 4|w(x)|^2]dx. \tag{5}$$

The system also conserves the momentum and Hamiltonian, which will not be explicitly used in this work.

We will start by studying the CW (continuous wave) solutions to Eqs. (1)–(3). These are sought for in the form of

$$u(z,x) = e^{ikz}A, \quad v(z,x) = e^{ikz}B, \quad w(z,x) = e^{2ikz}C, \tag{6}$$

where $A$, $B$, and $C$ are real constants that satisfy a system of cubic equations,

$$-(k-b)A + BC + \gamma\left(\tfrac{1}{4}A^2 + \tfrac{1}{4}B^2 + 2C^2\right)A + \tfrac{1}{6}\gamma C^2 B = 0, \tag{7}$$

$$-(k+b)B + AC + \gamma\left(\tfrac{1}{4}B^2 + \tfrac{1}{4}A^2 + 2C^2\right)B + \tfrac{1}{6}\gamma C^2 A = 0, \tag{8}$$

$$-(4k+q)C+AB+2\gamma(2C^2+A^2+B^2)C+\tfrac{1}{3}\gamma ABC=0. \tag{9}$$

A detailed study of the CW solutions is performed in Sec. III.

Next, we will seek for stationary soliton solutions in the form

$$u(z,x)=e^{ikz}U(x), \quad v(z,x)=e^{ikz}V(x), \quad w(z,x)=e^{2ikz}W(x), \tag{10}$$

where the real propagation constant $k$ is an intrinsic parameter of the soliton family, and the functions $U$, $V$, and $W$ may be assumed real too. The substitution of Eq. (10) into Eqs. (1)–(3) generates a system of ODEs (recall we have set $6\gamma_2=\gamma_1\equiv\gamma$ and $b\equiv 1$),

$$-(k-1)U+\tfrac{1}{2}U''+VW+\gamma\left(\tfrac{1}{4}U^2+\tfrac{1}{4}V^2+2W^2\right)U+\tfrac{1}{6}\gamma W^2 V$$
$$=0, \tag{11}$$

$$-(k+1)V+\tfrac{1}{2}V''+UW+\gamma\left(\tfrac{1}{4}V^2+\tfrac{1}{4}U^2+2W^2\right)V+\tfrac{1}{6}\gamma W^2 U$$
$$=0, \tag{12}$$

$$-(4k+q)W+\tfrac{1}{2}W''+UV+2\gamma(2W^2+U^2+V^2)W+\tfrac{1}{3}\gamma UVW$$
$$=0, \tag{13}$$

with the prime standing for $d/dx$. Fundamental solitons, which are the subject of the present work, are single-peaked even functions of $x$ vanishing at $x=\pm\infty$.

For soliton solutions, the power defined as per Eq. (5) is a function of $k$. The form of the function $E(k)$ is important, as the VK criterion [15] states that a necessary (but, generally speaking, not sufficient) condition for the stability of the soliton is given by

$$dE/dk>0. \tag{14}$$

Equations (11)–(13) admit obvious reductions to a single equation by setting $V=W=0$, or $U=W=0$, or $U=V=0$. The remaining equation takes the form, respectively,

$$-(k-1)U+\tfrac{1}{2}U''+\frac{\gamma}{4}U^3=0, \tag{15}$$

$$-(k+1)V+\tfrac{1}{2}V''+\frac{\gamma}{4}V^3=0, \tag{16}$$

$$-(4k+q)W+\tfrac{1}{2}W''+4\gamma W^3=0. \tag{17}$$

Exact soliton solutions to these equations are obvious:

$$U_{\text{slow}}=2\sqrt{\frac{2(k-1)}{\gamma}}\operatorname{sech}[\sqrt{2(k-1)}x], \tag{18}$$

$$V_{\text{fast}}=2\sqrt{\frac{2(k+1)}{\gamma}}\operatorname{sech}[\sqrt{2(k+1)}x], \tag{19}$$

$$W=\sqrt{\frac{4k+q}{2\gamma}}\operatorname{sech}[\sqrt{2(4k+q)}x], \tag{20}$$

provided that $\gamma>0$ and $k\mp 1>0$, or $4k+q>0$ (otherwise, these simple solitons do not exist).

The solutions (18) and (19) are also valid in the framework of the two-component $\chi^{(3)}$ model, in which Eq. (3) is dropped, and the variable $w$ is set equal to zero in Eqs. (1) and (2). A well-known result [12] is that, in the latter model, the soliton (18), which is called a slow one, is stable, and the soliton (19), which is called fast, is unstable. However, it is not immediately obvious whether or not these solitons are stable as particular solutions to the full system (1)–(3); this issue will be investigated below.

Note that the calculation of the power of the solutions (18) and (19) as per the definition (5) yields

$$E_{\text{slow,fast}}=(8/\gamma)\sqrt{2(k\mp 1)}. \tag{21}$$

From here, we see that both expressions (21) satisfy the VK criterion (14). Actually, in most cases the fast solitons are clearly unstable, due to a mechanism different than what the VK criteria addresses. This notwithstanding, the fast solitons do appear to be stable in some cases, see below. As for the slow solitons, it will be shown that they may be both stable and unstable in the present model, in drastic contrast with the above-mentioned $\chi^{(3)}$ system, where they are always stable.

As concerns the single-component solution (20), it might be expected that the $\chi^{(2)}$ nonlinearity makes it unstable against FF perturbations (i.e., small perturbations in the $u$ and $v$ components will mutually amplify each other). In most cases, this expectation is corroborated by direct simulations; nevertheless, a parameter region will be found where the SH solitons (20) are *stable*.

## III. CW SOLUTIONS

Our first objective is to study the CW solutions, which are to be found from Eqs. (7)–(9). For these solutions, the power is defined not by the integral expression (5), but rather as the corresponding density,

$$P=A^2+B^2+4C^2. \tag{22}$$

Note that Eqs. (7)–(9) are invariant with respect to the simultaneous reversal of the signs of $A$ and $B$, while the sign of $C$ is kept fixed. Therefore, in what follows below, we do not distinguish between solutions that may be transformed into each other this way.

Taking linear combinations of Eqs. (7) and (8), one can solve for $AB$ and $A^2+B^2$ in terms of $k$ and $C$. Then, inserting these results into Eq. (9), one can find $k$ as a function of $C$, hence, eventually, $A$ and $B$ can also be found as functions of $C$. In the process, one has to solve two quadratics, thus there are two signs to choose, giving a total of *four* different branches of the CW solutions. In selecting the possible signs, it is necessary to ensure that the final values for $A$, $B$, and $k$ are real. Each branch can meet this condition, giving rise to a family of physical solutions.

Stability of the CW solutions was studied against perturbations that also belong to the CW class, i.e., $x$-independent
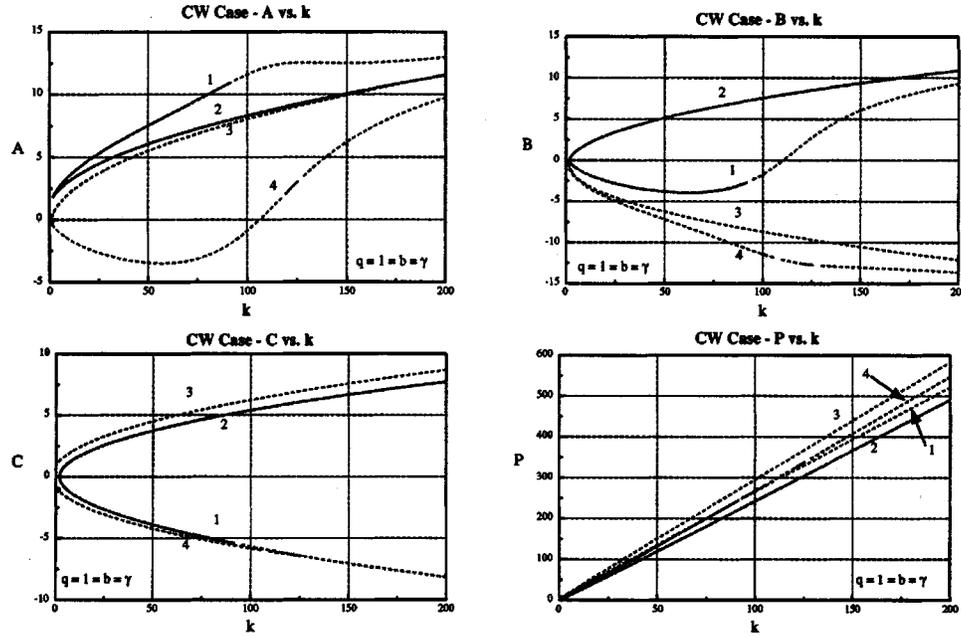
FIG. 1. The amplitudes $A$, $B$, $C$, and power density $P$ vs $k$ for the CW solutions, in the case of $b=q=\gamma=1$. The continuous and dashed lines represent stable and unstable solutions, respectively.

ones; from the viewpoint of the underlying equations (1)–(3), this of course implies only a necessary stability condition, as possible modulational instability against $x$-dependent perturbations is ignored in this section. To study the CW stability, we took perturbed solutions in the form of

$$u(z) = e^{ikz}[A + a_1(z) + ia_2(z)],$$

$$v(z) = e^{ikz}[B + b_1(z) + ib_2(z)],$$

$$w(z) = e^{2ikz}[C + c_1(z) + ic_2(z)], \qquad (23)$$

where $a_1$ through $c_2$ are real functions defining infinitesimal perturbations. They are sought for as

$$a_{1,2}(z) = a_{1,2}^{(0)}e^{\sigma z}, \quad b_{1,2} = b_{1,2}^{(0)}e^{\sigma z}, \quad c(z) = c_{1,2}^{(0)}e^{\sigma z}, \quad (24)$$

$\sigma$ being an instability growth rate. Substitution of Eqs. (24) into the linearized Eq. (1)–(3) yields a sixth-order algebraic equation for $\sigma$. The (CW-)stability condition amounts to the demand that the inequality Re $\sigma \leq 0$ must hold simultaneously for all the roots of this equation.

Equations (7)–(9) were solved not only in the indirect analytical form as described above, but also in a direct numerical fashion. A conclusion following from the numerical solution is that, as it could be expected, four different CW families are found for fixed $q$ and $\gamma$. A typical example of the solution families is shown in Fig. 1, for the case of $q=\gamma=1$ (recall we have also set $b=1$), the amplitudes $A$, $B$, $C$, and the power density $P$ [see Eq. (22)] being plotted versus $k$ (for $k>0$). The plots also show the stability of the CW solutions, predicted as described above from the calculation of the eigenvalues $\sigma$.

As one can see in Fig. 1, at small values of $k$ the amplitudes roughly follow a pattern of $\pm\sqrt{k}$ (the $\sqrt{k}$ dependence is expected when the SHG terms dominate). At larger $k$, two of the branches, one for $A$ and one for $B$, are seen to cross zero at different values of $k$. This behavior is due to a strong interplay of the $\chi^{(2)}$ and the $\chi^{(3)}$ nonlinearities occurring in this region. CW solutions also exist for $k<0$, but further consideration demonstrates that they all are unstable (see below), therefore the solutions for $k<0$ are not displayed here.

The four branches of the CW solutions can be classified as follows. Branch 1 is seen to be stable up to about $k \approx 100$. It is the branch along which the amplitude $B$ crosses zero. Branch 2 seems to be stable for all $k$, while branch 3 is unstable for all $k$. Branch 4 has a small segment of stability near $k \approx 150$, but otherwise appears to be unstable. It is the branch along which the amplitude $A$ crosses zero.

In the plot of $P$ in Fig. 1, one notes that the slopes of the power curves along all the branches is positive (and essentially constant). Thus the VK criterion does not stipulate any part of these branches to be unstable, unlike the direct stability analysis based on the calculation of the eigenvalues $\sigma$. In terms of energy considerations, we would expect branch 2 to be stable, as it always has the lowest power density for a given $k$. Indeed, this branch is always stable.

In many cases, the stability inferred from evaluating the eigenvalues $\sigma$ as described above, correlates to the sign of the SHG term in the system's Hamiltonian, which is

$$H_{SHG} = -ABC. \qquad (25)$$

Stable solutions are the ones which have $ABC>0$, wherein the SHG part of the Hamiltonian is negative, and unstable solutions have $ABC<0$. This conclusion is a very natural one, as stable solutions tend to minimize the Hamiltonian [16]. Looking at the plots for the CW solutions, we see that

this criterion is true for branches 2 and 3, and is true almost everywhere for branch 1. We also note that, in the plot of $B$ in Fig. 1, there appears to be a short segment of branch 1 where $B$ is negative, that by the Hamiltonian criteria, should be stable. But instead of being stable, this segment tests out as unstable. However, branch 4 does not obey the criterion based on the sign of the term (25), in that it would have to be stable in the entire region where $A > 0$, which is $k \gtrsim 110$, but, in reality, only a small stability segment is found near $k \approx 150$; otherwise, this branch tests out as an unstable one. This finding stresses that the condition of the negativeness of the Hamiltonian term (25) is only necessary, but not sufficient, for the stability.

CW solutions were also investigated in the case of the self-defocusing $\chi^{(3)}$ nonlinearity, with $\gamma < 0$. For instance, in the case of $\gamma = -0.05$ and $q = b = 1$, two branches of the solutions are stable and two are unstable. The stable branches all have $k < -1$ in this case, which implies that they have no soliton counterparts, since (regular) solitons may only exist for $k > 1$, see below. The unstable CW branches do have parts with $k > 1$, where solitons are possible. These results conform to the findings reported below, according to which all the solitons are unstable at $\gamma < 0$.

## IV. THE VARIATIONAL APPROXIMATION FOR THE 3W SOLITONS

In the presence of the $\chi^{(2)}$ nonlinearity only, VA turned out to be an efficient tool for the analysis of 3W solitons supported by the type-II SHG generation [20], which strongly suggests to apply VA to the present model as well. To this end, we note that the Lagrangian density from which the underlying Eqs. (1)–(3) can be derived is

$$
\mathcal{L} = \frac{1}{2}(iu^* \partial_z u + iv^* \partial_z v + 2iw^* \partial_z w + \text{c.c.}) + \frac{1}{2}\left(\left|\frac{du}{d\tau}\right|^2 + \left|\frac{dv}{d\tau}\right|^2\right)
$$

$$
+ \left|\frac{dw}{d\tau}\right|^2\right) + b(|u|^2 - |v|^2) - q|w|^2 + (u^*v^*w + w^*uv)
$$

$$
+ \frac{\gamma}{8}(|u|^4 + |v|^4) + 2\gamma(|u|^2 + |v|^2 + |w|^2)|w|^2 + \frac{\gamma}{6}(|u|^2|v|^2
$$

$$
+ u^*v|w|^2 + v^*u|w|^2) + \frac{\gamma}{24}[(u^*v)^2 + (v^*u)^2], \tag{26}
$$

where c.c. stands for the complex conjugate expression.

In this work, we adopt the Gaussian ansatz for the soliton trial functions. Of course, it incorrectly approximates far tails of the soliton, which must decay exponentially, rather than Gaussian-like. But in the one-dimensional case, this factor is not crucially important [14]. Moreover, we assume that all the three components of the solitons have identical widths (an ansatz with different widths can be introduced, but it gives rise to an extremely cumbersome algebra). In any case,

the latter assumption is not a serious limitation on the applicability of the VA, since direct numerical results show that almost all the soliton solutions do have approximately equal widths, except when $k$ is near the edge of the continuous spectrum.

Thus, the variational ansatz is taken as

$$
u, v, w = A_{u,v,w} \exp[-(\tau^2/\rho^2) + i\alpha_{u,v,w}], \tag{27}
$$

where $A_{u,v,w}$ are real amplitudes, $\rho$ is the common width, and $\alpha_{u,v,w}$ are phases at the center of the respective component. Inserting the ansatz (27) into the Lagrangian density (26), one can calculate the *effective Lagrangian*,

$$
L_{\text{eff}} \equiv \int_{-\infty}^{+\infty} \mathcal{L}(x)dx = -\sqrt{\frac{\pi}{2}}\rho(A_u^2 \dot{\alpha}_u + A_v^2 \dot{\alpha}_v + 2A_w^2 \dot{\alpha}_w)
$$

$$
- \sqrt{\frac{\pi}{2}}\left[\left(q\rho + \frac{1}{2\rho}\right)A_w^2 + \left(b\rho + \frac{1}{2\rho}\right)A_v^2\right.
$$

$$
- \left(b\rho - \frac{1}{2\rho}\right)A_u^2\right] + 2\sqrt{\frac{\pi}{3}}\rho A_u A_v A_w \cos(\alpha_u + \alpha_v - \alpha_w)
$$

$$
+ \sqrt{\pi}\rho\left[(A_u^2 + A_v^2 + A_w^2)A_w^2 + \frac{1}{16}\left(A_u^4 + \frac{4}{3}A_u^2 A_v^2 + A_v^4\right)\right]
$$

$$
+ \frac{1}{6}\sqrt{\pi}\rho[A_u A_v A_w^2 \cos(\alpha_u - \alpha_v)
$$

$$
+ \tfrac{1}{4}A_u^2 A_v^2 \cos(2\alpha_u - 2\alpha_v)], \tag{28}
$$

where the overdot stands for $d/dz$. Since we are only interested in stationary soliton solutions, we assume that all the components contain a single propagation constant, $\dot{\alpha}_u = \dot{\alpha}_v = \dot{\alpha}_w/2 \equiv k$. It is an intrinsic parameter of the soliton family, rather than a variational one, while $A_{u,v,w}$ and $\rho$ are four variational degrees of freedom. Then, the Euler-Lagrange equations $\partial L_{\text{eff}}/\partial A_{u,v,w} = \partial L_{\text{eff}}/\partial \rho = 0$ yield the following system:

$$
\left(\frac{1}{\rho^2} + 2(k-b)\right)\frac{A_u}{\sqrt{2}} - \frac{2}{\sqrt{3}}A_v A_w - \frac{\gamma}{4}A_u(A_u^2 + A_v^2)
$$

$$
- 2\gamma\left(A_u + \frac{A_v}{12}\right)A_w^2 = 0,
$$

$$
\left(\frac{1}{\rho^2} + 2(k+b)\right)\frac{A_v}{\sqrt{2}} - \frac{2}{\sqrt{3}}A_u A_w - \frac{\gamma}{4}A_v(A_u^2 + A_v^2)
$$

$$
- 2\gamma\left(A_v + \frac{A_u}{12}\right)A_w^2 = 0,
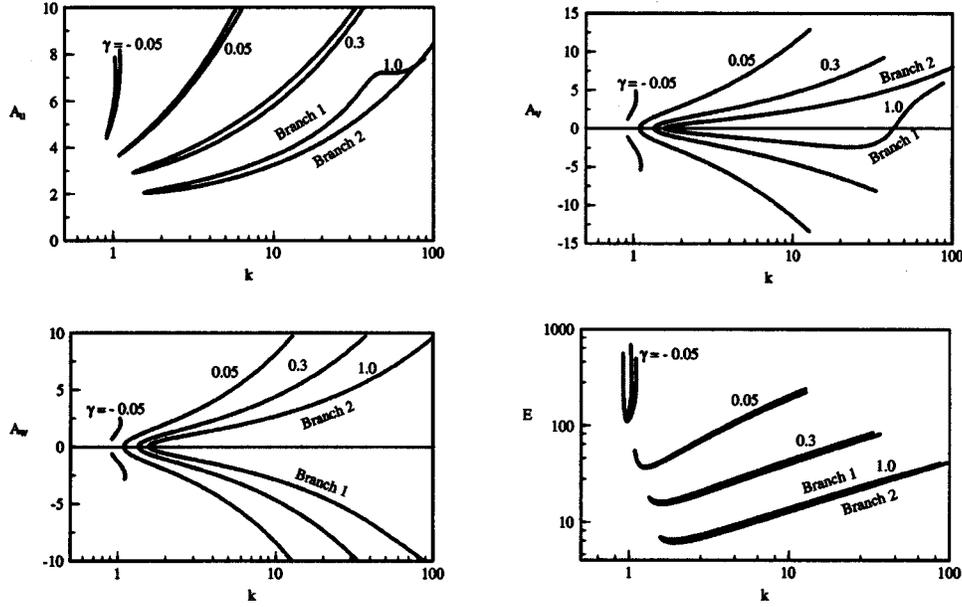$$

FIG. 2. The amplitudes of the three-wave soliton $A_u$, $A_v$, and $A_w$, and the power $E(k)$ as found from the variational approximation vs $k$ for the first two solution branches, when $q=b=1$.

$$\left(\frac{1}{\rho^2}+8k+2q\right)\frac{A_w}{\sqrt{2}}-\frac{2}{\sqrt{3}}A_uA_v-4\gamma A_w^3$$

$$-2\gamma\left(A_u^2++\frac{1}{6}A_uA_v+A_v^2\right)=0,$$

$$\left(b-k+\frac{1}{2\rho^2}\right)\frac{A_u^2}{\sqrt{2}}+\left(-b-k+\frac{1}{2\rho^2}\right)\frac{A_v^2}{\sqrt{2}}$$

$$+\left(-q-4k+\frac{1}{2\rho^2}\right)\frac{A_w^2}{\sqrt{2}}+\frac{2}{\sqrt{3}}A_uA_vA_w+\frac{\gamma}{16}(A_u^2+A_v^2)^2$$

$$+\gamma\left(A_u^2+\frac{1}{6}A_uA_v+A_v^2\right)A_w^2=0. \tag{29}$$

These equations feature close similarity to the CW Eqs. (7)–(9) derived above. In particular, as in the CW case, it is a set of coupled cubic equations, and due to the symmetries involved, we can solve these equations by using only two square roots, hence there are four possible solution branches.

We proceed by solving Eqs. (29) numerically. Typical examples of the solutions are presented in Fig. 2, where we show two solution branches, for $\gamma=-0.05, 0.05, 0.3$, and 1.0. This figure reveals two broad (in terms of the range of values of $k$) families of solutions. As a matter of fact, these two families are counterparts of the branches 1 and 2 in the CW case. In particular, one notes that, for $\gamma=1$ (the same value which was selected for the CW solutions in Fig. 1), the shape of each solution branch closely matches the corresponding solution in the CW case (note that the $k$ axis in the CW figures is linear, while in Fig. 2 it is logarithmic).

We stress that the variational solutions exist also for the defocusing $\chi^{(3)}$ nonlinearity, $\gamma<0$, although apparently only for rather small $|\gamma|$. In particular, for negative $\gamma$, the soliton solution also exists for $k<1$, i.e., for $k$ belonging to the

continuous spectrum of the linearized system. Thus, this sector of the solutions represents the above-mentioned delocalized solitons [17], and may possibly include embedded solitons [18].

In the same figure, we show the soliton's power $E=\rho(A_u^2+A_v^2+4A_w^2)$ [which is the power (22) calculated with the ansatz (27)] versus $k$. One notes here that, in the left parts of all these solution branches, the curves have a negative slope. Thus, by the VK criterion, the solutions should be unstable in this case. Numerical simulations of the full system (1)–(3) (see the following section) verify this prediction for the truly localized solutions.

Two other families of the variational solutions for the solitons are shown in Fig. 3. In this case, we clearly see a family which is a counterpart of branch 4 of the CW solution. However, the variational solutions for $\gamma=1.0$ do not contain a counterpart of the CW branch 3 (note, however, that branch 3 in the CW case was completely unstable). Nevertheless, that branch reappears at lower values of $\gamma$, and we have plotted it for $\gamma=0.3$.

In addition, we also note the presence of another branch which was not found in the CW case. It appears in the plot for $A_v$ in Fig. 3 as a very short branch near the bottom for $\gamma=0.3$. Actually, it is just another segment of branch 3, which exists only at finite values of the soliton's width $\rho$ (the CW solutions correspond to $\rho=\infty$, that is why this segment was not found among the CW states). Note that $A_w$ may be regarded as an internal parameter of the family of these solutions, and the latter segment is found in a range of $A_w$ which, in the CW case, did not produce a solution for branch 3. There is also a separate segment near zero for $\gamma=0.05$, which is clearly a continuation of branches 3 and 4 for that value of $\gamma$.

The solutions for $\gamma=0.05$ and $\gamma=0.3$ are also found to exist for $k<1$ (inside the continuous spectrum), and large parts of the solution for $\gamma=0.05$ extend even to $k<0$. The
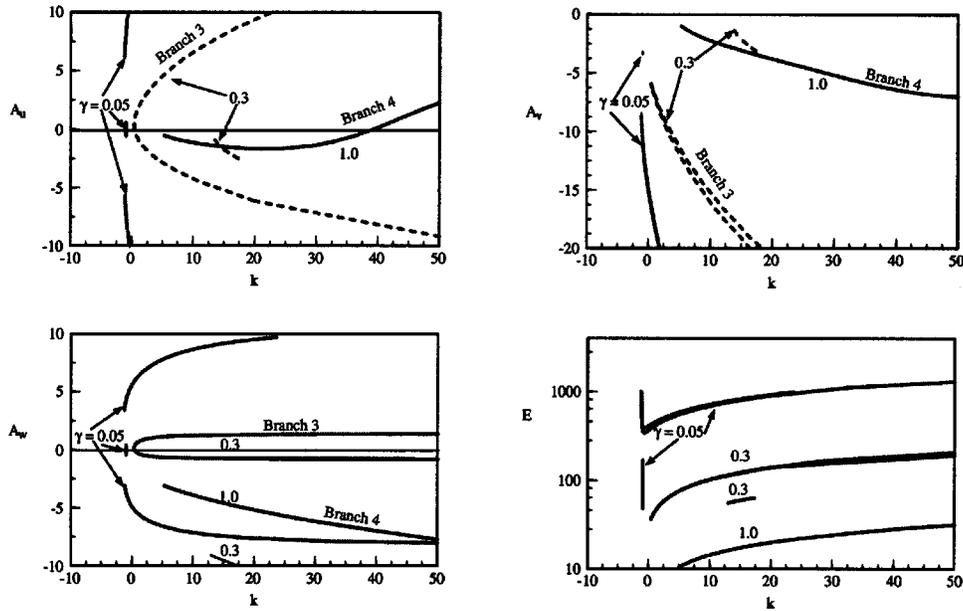
FIG. 3. The same as in Fig. 2 for the other two branches.

solutions in these ranges again correspond to delocalized solitons (and, possibly, to embedded ones).

In Fig. 3, we also show $E$ versus $k$ for these solutions. As is seen, for $k>1$ all the slopes are positive, hence these sections are stable by the VK criteria. It is clear from this plot that the two families are distinctly different.

In the first plot in Fig. 4, we show the soliton's width $\rho$ as a function of $k$ for the first two branches. A noteworthy feature evident in this plot is a *universal dependence* of the width versus $k$, which is insensitive to $\gamma$. Another feature of importance is that $\rho$ does become very large, and in fact appears to be going toward infinity, for the solutions with $k<1$ (in the delocalized-soliton range). This is what one would expect for a localized object with an infinitely long tail, and is the best fit that the VA can produce, when restricted to the Gaussian approximation. We note that a more sophisticated ansatz, combining the Gaussian approximation for the core of the (weakly) delocalized solitons, and a cosine-based ansatz for the oscillating tails, makes it possible to pin (with good accuracy) a truly localized ES (embedded soliton) inside the family of the delocalized ones [21] (a similar variational ansatz, combining the sech approximation for the core of the soliton, and a long shelf approximating its

tail, was earlier used in a different context, in order to describe emission of radiation by a perturbed soliton [22]). However, search for ESs in the present model is beyond the scope of this work.

The second plot in Fig. 4 shows, for the soliton solutions from Fig. 3, their width versus $k$. Here, for $\gamma=0.05$, we note that $\rho$ again diverges at small $k$. Note a principal difference from the previous plot: this time, the curves $\rho(k)$, obtained for different values of $\gamma$, do *not* approximately collapse into a single one.

The VK criterion predicts that branches 1, 2, and 4 of the soliton solutions should have exactly the same stability as their CW counterparts, in the respective sectors. The new branch of the large-amplitude solitons found at small positive $\gamma$ (in particular, for $\gamma=0.3$) is expected to be always unstable, since $A_u$, $A_v$, and $A_w$ all are negative, making the SHG Hamiltonian term (25) positive for these solitons. Numerical simulations of the full system of Eqs. (1)–(3) readily verify this conjecture.

## V. NUMERICAL RESULTS

In this section, we will first find the 3W solitons in a numerically exact form by solving the two-point boundary-
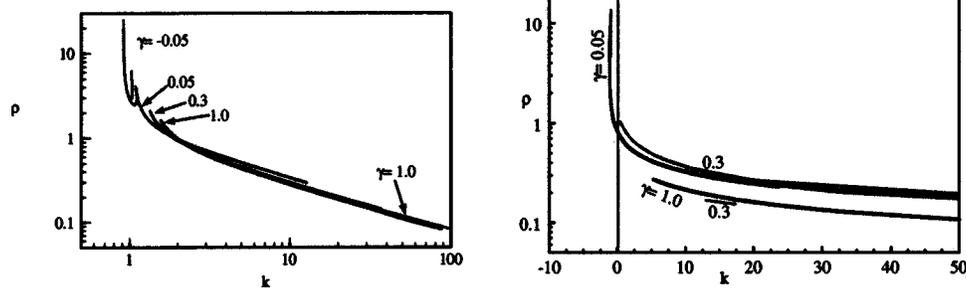


FIG. 4. The variational solutions for the width of the soliton $\rho$ vs $k$, when $q=b=1$. The results for the first two branches are on the left, and those for the last two branches are on the right.

value problem for Eqs. (11)–(13), using the collocation method [23]. In the computations of Eqs. (1)–(3), the spectral method was used for the space discretization, and the leap-frog method for advancing in $z$.

As an initial wave form, we used particular exact solutions

$$U = (3k/2)\text{sech}^2(\sqrt{2k}x/2), \tag{30}$$

$$V = W = U, \quad V = W = -U, \quad V = -W = U, \quad V = -W = -U, \tag{31}$$

which are available in the case with

$$\gamma = 0, \quad b = 0, \quad k > 0, \quad q = -3k. \tag{32}$$

Starting from here, soliton solutions for other values of the parameters were found by continuation. Of course, this approach comes with a risk of missing soliton families that do not abut onto the simple solutions (31) as the parameters approach the special values (32). However, the VA results, and comparison with the CW solutions suggest that, following this procedure, we have not missed other soliton families. An exception is branch 5 of the soliton solutions, which is presented below: it, indeed, cannot be generated by the above method. This branch was found as a result of an additional exploration of the parameter space, with the aim to search for possibly missing solution families.

In order to distinguish between various branches of the soliton solutions, we took advantage of the fact that each component of the fundamental soliton keeps a definite sign [and the relation between the signs is quite important for the stability of solitons, as is suggested by the Hamiltonian term (25)]. Thus, we have adopted a notation based on the signs of the $u$, $v$, and $w$ components: branches obtained by the continuation of four distinct types of the solutions singled out in Eq. (31) will be designated by symbols $PPP$, $PNN$, and so on, where $P$ and $N$ stand for the positive or negative sign of each component $u$, $v$, $w$.

To test stability of soliton solutions, we simulated their evolution within the framework of the full system of Eqs. (1)–(3), adding a small perturbation to a given stationary soliton $[U(x), V(x), W(x)]$. To this end, various perturbations were used—in particular, those proportional to $\epsilon[|U(x)| + |V(x)| + |W(x)|]$ rand $(x)$, where $\epsilon$ is a small amplitude of the perturbation and rand$(x)$ is a random function taking values in the interval $(0,1)$. As a result, we have concluded that this random perturbation always leads to precisely the same conclusion concerning stability/instability of the unperturbed soliton as a simpler perturbation, defined so that the initial field configuration is deformed to

$$(u,v,w)_0 = (U,V,W) + \epsilon(|U| + |V| + |W|), \tag{33}$$

which will be used in typical examples displayed below. As mentioned above, if $[U(x), V(x), W(x)]$ is a stationary solution to Eqs. (11)–(13), then $[-U(x), -V(x), W(x)]$ is a solution too. Therefore, without loss of generality, we always take $U(x=0) \geq 0$.

## A. Validation of the variational approximation

First, we compare the numerical solutions against the results furnished by the VA. It has been concluded that the VA solutions are always qualitatively correct, and are also approximately correct in the quantitative sense. Some examples are sufficient to make this point.

The first example is the numerically found families of soliton solutions to Eqs. (11)–(13) for $q=1$ and $\gamma=-0.01$ or 1, which are presented in Fig. 5. In this figure, the soliton's amplitudes, $(U_{max}, V_{max}, W_{max}) \equiv [U(x=0), V(x=0), W(x=0)]$, are plotted versus $k$, along with the power $E(k)$ which is defined as per Eq. (5). Comparing branch 1 and branch 2 in these graphs against their VA counterparts displayed in Figs. 2 and 3, it is clear that the VA offers a correct qualitative description of the soliton solutions. In particular, the branch in Fig. 5 labeled "branch 5," which is the numerical solution for $\gamma=1$, does correspond to the short segment predicted for $\gamma=0.3$ by the VA in Fig. 3, which is labeled there as branch 3. So, it appears that the section labeled as branch 5 in Fig. 5 is nothing else than a section of the VA solution labeled as branch 3. However, for $\gamma=1$ (unlike $\gamma=0.3$), this VA solution did not exist, which is explained by the fact that, as the exact numerical solution shows, the width of the $W$ component is much smaller than that of the other two components, in violation of the equal-widths assumption implied in the variational ansatz (27). Since the VA did find this branch for $\gamma=0.3$, we may still infer that the VA produces qualitatively correct results, even if not quantitatively accurate, in some cases. Other examples support this point as well.

As concerns the continuation of the soliton solutions to $\gamma < 0$, at $k=2$ the numerical solution of the $PPP$ type, by which we mean the one with $U(0)>0, V(0)>0, W(0)>0$, terminates at (does not continue below) $\gamma=-0.027$. On the other hand, the VA has found such solutions existing up to $\gamma=-0.05$ (see Fig. 2). So, in this case again, the qualitative predictions of the VA are correct, and the quantitative difference is not too large.

Further evidence can be produced, to demonstrate that the numerical findings for branches 3 and 4 of the soliton solutions, and for other values of $\gamma$ verify the qualitative accuracy of the VA, and its generally good quantitative agreement with the numerical results. Thus, the VA applies to the 3W solitons in the $\chi^{(2)}:\chi^{(3)}$ model, as well as it did in the vectorial $\chi^{(2)}$ one [20].

## B. Stability of the single-component solitons

Now we proceed to the stability of the simple single-component soliton solutions, which are given by Eqs. (18)–(20). We start with the $U$ soliton (18), alias the slow one, which is always stable in the two-wave $\chi^{(3)}$ model [12]. Numerical tests conclude that, in the present system, the slow soliton has its stability *and instability* regions. The soliton is considered to be stable if the perturbed solution remains close to the original soliton, as long as the perturbation amplitude $\epsilon$ is small [see Eq. (33)], so that with the decrease of $\epsilon$ the perturbed soliton gets closer to the original one. Figure 6 demonstrates that the slow solitons are stable for
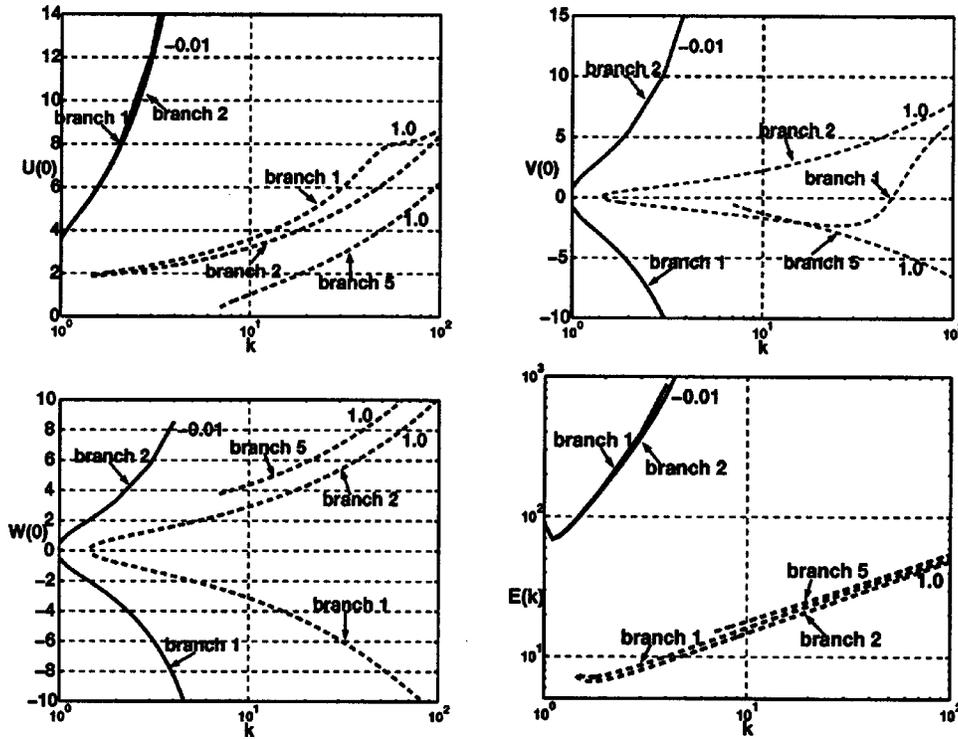
FIG. 5. Numerically found amplitudes and power of the three-wave solitons for $b=q=1$.

most of the $q$ values except when $23 \leq q \leq 26$ and $35 \leq q \leq 41.2 \equiv q_U$ for $k=5$ (the meaning of $q_U$ is explained below).

The transition between stable and unstable solitons of the $U$- (slow) type may seem differently. For example, the transition at $q \approx 26$ is smoother than at $q=q_U$. As $q$ approaches the transition point $q=26$ from below, the breather (which replaces the unstable soliton) gradually becomes closer to the unperturbed slow soliton (the amplitude of the breather's oscillations decreases), and finally the soliton becomes stable. But as $q$ passes the value $q_U$ at the above-mentioned transition point $q=q_U$, the perturbed soliton is quickly transformed into a breather, which is significantly different from the unperturbed slow soliton. Similar observations were made at other values of $k$.

The stability of the single-component SH ($W$) soliton (20) is also shown in Fig. 6 for $k=5$. An upper part of this branch

[in the region of $W(x=0) \geq 4.7$] was dropped after it has become unstable, as it never restabilizes, and, if continued, it makes the entire bifurcation diagram (which is further explained in the following section) rather obscure due to ostensible intersections with other branches. Thus, the single-component SH solitons exist only if $q > -4k$; most of them are unstable, except when $-4k < q < q_W \equiv -12$, and when $2 < q < 5$.

In fact, the character of the stability in the latter short interval is not quite clear. For a given initial perturbation with an amplitude $\epsilon$, the difference between the perturbed solution, as produced by the simulations, and the original soliton is almost proportional to $\varepsilon$, which suggests that the soliton is stable. A slight growth on the deviation from that behavior was observed too, but, since the deviation was very small, we classify the SH soliton to be stable in this case.
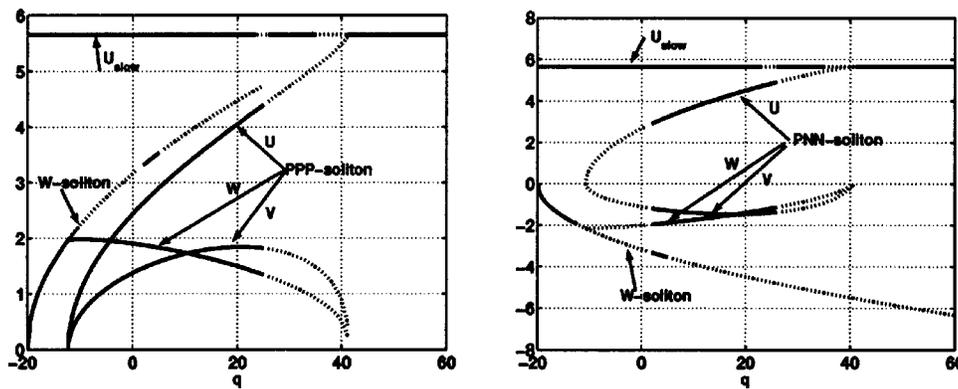


FIG. 6. Stability regions of the single-mode $U$-(slow) and $W$-(SH) solitons, and three-mode $PPP$ and $PNN$ solitons for $k=5, b=\gamma=1$. Nonzero amplitudes of the solitons, i.e., $U(x=0), V(x=0)$, and $W(x=0)$, are shown as functions of the mismatch $q$.
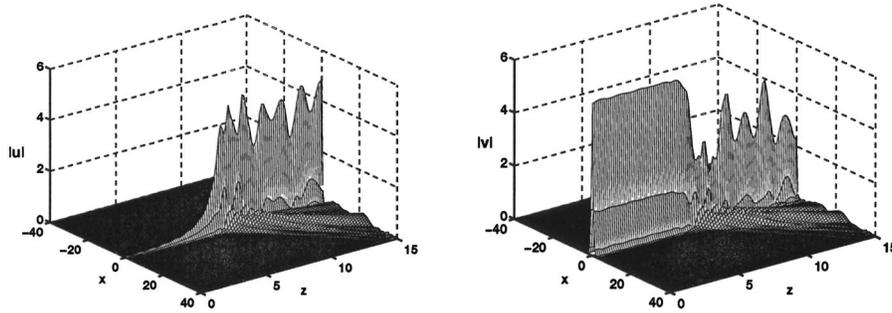
FIG. 7. An example of the transformation of an unstable $V$ (fast) soliton into a breather, in the case of $q=29$, $k=3$, and $\epsilon=0.01$. The behavior of $|w|$ is similar to that of $|u|$.

Even with these reservations, the observation of the SH soliton which is *stable* against the FF perturbations appears to be quite a noteworthy result, as it was commonly believed that such solitons can never be stable.

The stability test of the single-component $V$ soliton [the fast one, see Eq. (19)] demonstrates that it is almost always unstable, as shown in the example displayed in Fig. 7 for $q=29$ and $k=3$. The instability sets in somewhat faster for $\epsilon>0$ than for negative $\epsilon$ [see Eq. (33)] in this case. In both cases, the eventual result is transformation of the unstable soliton into an apparently stable breather. Established values of the amplitude and frequency of the breather's intrinsic oscillations do not depend on the sign and size of the perturbation amplitude $\epsilon$ (provided that it is not too large). Generally, the established state of the breather has its amplitude in the $u$ and $w$ components comparable to that of $v$.

It is noteworthy that, despite the expected (from the comparison with the well-known results for the $\chi^{(3)}$ model [12]) instability of the $V$ soliton in a bigger part of the parameter space, we did observe, for instance at $k=5$, that it is *stable* for $60<q<64$. As this stabilization is not related to any apparent bifurcation, one might conjecture that, in this interval, the $V$ soliton remains formally unstable, but its instability is, for some specific reason, extremely weak; then, for physical applications, it is a real stability interval anyway.

Besides that, it is also noted that the instability of the $V$ soliton develops, if any, extremely slowly for very broad solitons, with a small value of $k+1$. This feature is quite natural, as the amplitude of the soliton is very small in this case.

### C. The main family of three-wave solitons: the *PPP* type

To present numerical results for the solitons in the general case, with all the three components present, we first focus on the case of $\gamma=1$. By starting from the exact solution (31) with $V=W=U$, then numerically continuing it from $b=\gamma=0$ to $b=\gamma=1$, and after that varying the parameters $k$ and $q$, we were able to find solitons with positive stationary fields, $U(x)>0, V(x)>0, W(x)>0$, in a large range of $k$ and $q$, which is shown in Fig. 8(a). According to the nomenclature introduced above, these solitons are of the *PPP* type.

For any fixed $q$, this branch of the soliton solutions exists if $k$ is larger than a critical value. Further analysis of the numerical data demonstrates that the existence region of the

branch in the $(k,q)$ plane can be approximated by

$$q_W = -2.05(k-1) - 4 < q < q_U = 11.3(k-1) - 4.$$

(34)

As $q$ approaches $q_U$, the $UVW$ soliton (the general 3W one) of the *PPP* type *bifurcates into* the slow $U$ soliton (18), and as $q$ gets larger than $q_W$, the $UVW$ soliton *bifurcates from* the $W$ soliton (20). Note that the $U$ soliton exists for $k>1$ and any $q$, and the $W$ soliton exists for $q>-4k$. Therefore, in the region (34), where the main 3W soliton branch exists, the $U$ and $W$ solitons exist too. Thus, the $UVW$ family actually provides for a crossover between the stable $U$- and unstable $W$-soliton branches.

To illustrate the crossover, the amplitudes $[U(x=0), V(x=0), W(x=0)]$ of the $UVW$ soliton are plotted in Figs. 6 and 8(b) for the fixed values of the propagation constant, $k=6.4$ and $k=5$, respectively. As $q$ increases, $U(x=0)$ monotonously increases from 0, while $W(x=0)$ monotonically approaches zero. Simultaneously, the amplitude $V(x=0)$ increases from zero to some maximum value, and then decays back to zero.

The amplitudes of the $UVW$ solitons are also plotted against $k$, for two fixed values of the mismatch, $q=-6$ and $q=4$, in Figs. 8(c) and 8(d). As $k$ increases, $U(x=0), V(x=0)$, and $W(x=0)$ increase too. With respect to Fig. 8(a), Figs. 8(b)–8(d) and Fig. 6 actually show the amplitudes of the solitons along vertical cuts at $k=6.4$ and $k=5$, and along horizontal cuts at $q=-6$ and $q=4$.

Stability of the soliton solutions is the most important issue. Therefore, the power function $E(k)$ defined in Eq. (5) is also plotted in Figs. 8(c) and 8(d), with the intention to apply the VK criterion. From the latter plots we see that, for $q=4$, the criterion for the $UVW$ soliton to be stable, $dE(k)/dk>0$ [see Eq. (14)], does not hold at $k<k^* \approx 2.2$. The dashed line in Fig. 8(a) separates the region $dE(k)/dk>0$ from the region $dE(k)/dk<0$, where the solitons are unstable. We note that this presumably unstable region of the $UVW$ soliton is the one with small $V$ and $W$ components.

Then, the stability of the solitons along the line $q=4$ was tested in direct simulations, starting with a stable $U$ soliton. For $k$ in the region where the condition (14) is violated, the $UVW$ solitons are found to be unstable indeed, as predicted
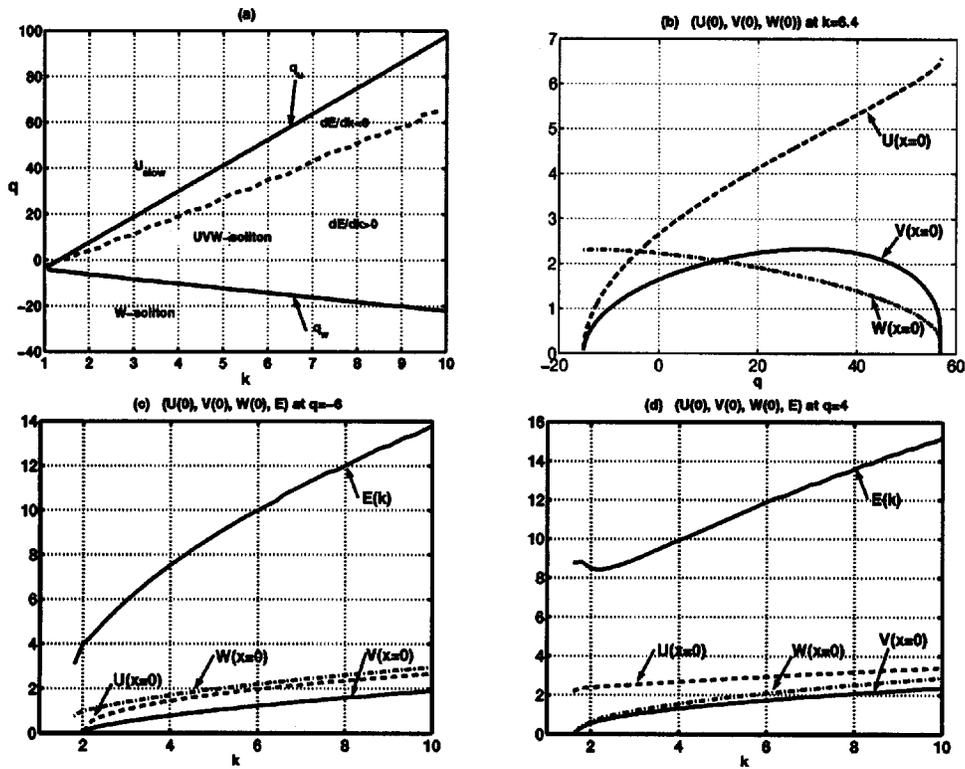
FIG. 8. (a) The *UVW* solitons of the *PPP* type exist between $q_w$ and $q_u$. In the region where $dE/dk < 0$, the solitons are unstable. (b) Amplitudes of the *UVW* soliton $U(x=0), V(x=0), W(x=0)$ for $k=6.4$. (c) and (d) Amplitudes and power of the *UVW* soliton $U(x=0), V(x=0), W(x=0)$, and $E$ for $q=-6$ and $q=4$, respectively.

by the VK criterion, see Fig. 8(d). As a typical example, the evolution of the unstable soliton is displayed in Fig. 9 for $k=1.8, q=4$. The simulations are conducted without imposing any perturbation [i.e., $\epsilon=0$ in Eq. (33)], the truncation error of the numerical scheme triggering the instability. Initially, the magnitudes of the fields $v$ and $w$ are small in comparison with $u$. Energy is then transferred between the components periodically, i.e., the instability does not destroy the soliton, but transforms it into a breather, as was also found in the previous unstable cases.
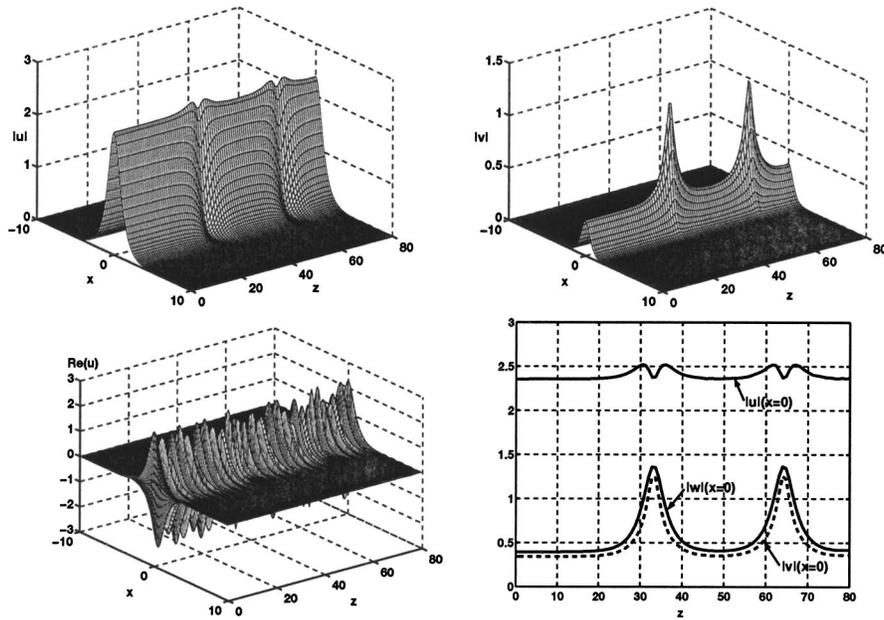


FIG. 9. Transformation of an unstable *UVW* soliton into a breather in the case of $k=1.8, q=4, \epsilon=0$. The behavior of $|w|$ is similar to that of $|v|$.

The stability tests were also run with an initially imposed perturbation $\epsilon > 0$. As $\epsilon$ increases, the breathers are formed earlier (after passing a shorter distance $z$), and the oscillation period $L$ of the established breather becomes smaller. For instance, $L \approx 19$ when $\epsilon = 0.02$, and $L \approx 30$ when $\epsilon = 0$, as shown in Fig. 9. The established amplitude of the oscillations weakly depends on $\epsilon$, being slightly smaller for $\epsilon = 0$ than in the case of $\varepsilon = 0.02$. The actual independence of the established amplitude on the size of the perturbation is a major criterion in deciding whether the soliton is unstable: for a *weakly stable* soliton, surrounded by a family of stable weakly excited breathers, the amplitude of the internal oscillations of the breather is expected to scale as a power of the perturbation amplitude $\epsilon$, while for a truly unstable soliton, the established amplitude, in the first approximation, should not depend on $\epsilon$.

Increasing $k$ further, the VK criterion (14) is met. In this case, a series of numerical simulations for the *UVW* soliton was carried out, varying $\epsilon$ while other parameters were kept constant. For instance, at $k = 2.5$ and $k = 10$ this was done for $\epsilon = 0.02, 0.01, 0.005$, and, finally, for $\epsilon = 0$. In this case, the initial perturbation also leads to a transition from the soliton to a breather. However, in contrast to the case when the soliton was unstable, this time we observed that, with the decrease of $\epsilon$, the breather's intrinsic frequency became smaller, and the amplitude of its oscillations *decreased* quite significantly with $\epsilon$ (almost linearly). Without adding the initial perturbation ($\epsilon = 0$), the original soliton is preserved, at least, for up to $z = 80$. Therefore, according to the above explanation, the solitons are indeed stable when the VK criterion is met. However, the numerical results strongly suggest that there are families of breathers quite close to the soliton solutions, and that small *finite* perturbations may provoke the transition of the soliton into a breather. In other words, the stable stationary soliton seems like a stable fixed point of the center type, which is surrounded by a family of closed trajectories, in a finite-dimensional Hamiltonian dynamical system.

In summary, moving along the line $q = 4$ and increasing $k$, we start with stable $U$ solitons, which change into unstable *UVW* solitons (the latter spontaneously evolve into breathers, in direct simulations). Later, the *UVW* solitons became stable, in accordance with the condition (14).

At $q = -6$, the VK condition (14) is *always* satisfied. Accordingly, the *UVW* solitons are found to be always stable in direct simulations in this case. The stability tests were also conducted along the line of $k = 5$, yielding the same result (see the first plot in Fig. 6). Thus, with regard to Fig. 8(a), we conclude that the *UVW* solitons (with $\gamma = 1$) are found to be stable in a larger part of the parametric space, except in a small strip near the upper boundary, where the magnitudes of $V$ and $W$ are small.

### D. Normal-form description of the bifurcations

Getting back to the bifurcations between the *UVW* soliton and its single-component $W$ and $U$ counterparts at the points $q = q_W$ and $q = q_U$, which are shown in Fig. 6 (the first plot for *PPP* type and second plot for *PNN* type), we have also investigated the stability of these solitons as they pass the bifurcation points. The plot for the *PPP* types demonstrates that, near the bifurcation point, the $W$ soliton is *stable* at $q < q_W$, and unstable at $q > q_W$. The $U$ soliton is unstable at $q < q_U$ and *weakly stable* at $q > q_U$. The latter means that it is stable against very small perturbations, but a slightly stronger disturbance triggers transition to a breather which is not close to the unperturbed $U$ soliton. For instance, at $\gamma = b = 1$ and $k = 5$, the stationary $U$ soliton found at $q = 41.2$ [which is very close to the bifurcation point $q = q_U$, see Eq. (34)] has the amplitude $U(x = 0) = 5.65$, and it is destabilized by the perturbation of the form (33) with $\epsilon \geq 0.005$ (while the soliton is certainly stable against the same perturbation with $\epsilon \leq 0.0025$); as a result, the $U$ soliton transforms into a breather whose oscillating amplitudes take values in the ranges, respectively, $4.8 < |u(x = 0)| < 6.0$, $2.6 < |v(x = 0)| < 4.6$, and $1.9 < |w(x = 0)| < 3.1$.

These features, together with the aforementioned stability of the *UVW* soliton at $q - q_W \rightarrow +0$ and its instability at $q - q_U \rightarrow -0$, call for derivation of normal forms [24] for the two bifurcations. Close to either bifurcation point, two components of the soliton (for instance, the $v$ and $w$ components near $q = q_U$) are small, which suggests to perform expansion in powers of the small fields. One may expect that the quadratic terms in the underlying Eqs. (1)–(3) will eventually combine into cubic ones, and the normal-form equations will therefore contain linear and cubic terms.

However, there is a difficulty in the course of the derivation. For instance, in the case when the $v$ and $w$ fields are small, Eqs. (2) and (3) in the linear approximation amount to a fourth-order ODE system with potential terms $\sim \mathrm{sech}^2[\sqrt{2(k-1)}x]$ [see Eq. (18)], and, additionally, cross-coupling terms $\sim \mathrm{sech}[\sqrt{2(k-1)}x]$; it is not straightforward at all to find exact eigenmodes of such a system, which is the first necessary step in the development of the bifurcation analysis. For this reason, we here put forward "phenomenological" normal forms, that we expect to be valid for the two bifurcations, while a consistent derivation will be presented elsewhere.

The normal form that can describe the bifurcation at the point $q = q_U$ includes dynamical equations for two variables $\xi_1(z)$ and $\xi_2(z)$,

$$\frac{d^2\xi_1}{dz^2} = -a_1\xi_1(\epsilon - b_1\xi_1^2 - c_1\xi_2^2), \tag{35}$$

$$\frac{d^2\xi_2}{dz^2} = -a_2\xi_2(\epsilon + b_2\xi_2^2 + c_2\xi_1^2), \tag{36}$$

where $\epsilon \equiv (q - q_U)/q_U$ is the bifurcation parameter, $a_{1,2}$, $b_{1,2}$, and $c_{1,2}$ being some positive constants. We stress that both Eqs. (35) and (36) contain the same control parameter $\epsilon$. As for the meaning of the variables $\xi_1$ and $\xi_2$, we conjecture that they are proportional to two linearly independent combinations of the amplitudes $V(x = 0)$ and $W(x = 0)$.

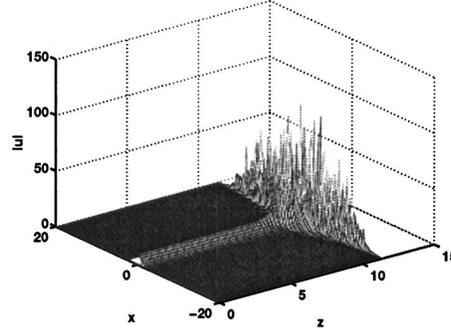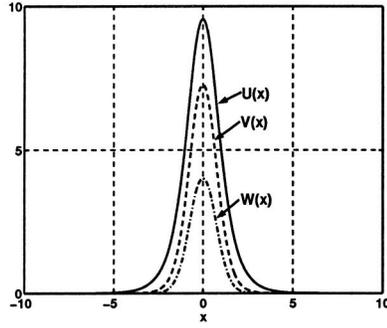Equations (35) and (36) give rise to the following fixed points (FPs):

FIG. 10. Evolution of an unstable $UVW$ soliton in the case of the self-defocusing $\chi^{(3)}$ nonlinearity, with $\gamma=-0.02, k=2, q=1, \epsilon=0$. The fields $|v|$ and $|w|$ behave similarly to $|u|$.

$$\xi_1^{(0)} = \xi_2^{(0)} = 0, \tag{37}$$

which corresponds to the $U$ soliton, and

$$\xi_1^{(+)} = \pm \sqrt{\epsilon/b_1}, \xi_2^{(+)} = 0 \text{ for } \epsilon > 0, \tag{38}$$

$$\xi_1^{(-)} = 0, \xi_2^{(-)} = \pm \sqrt{-\epsilon/b_2} \text{ for } \epsilon < 0, \tag{39}$$

which correspond to the solitons of the $UVW$ type. Assuming small perturbations around the FPs of the form $\exp(\gamma z)$, an elementary calculation yields the following stability eigenvalues:

$$[\gamma_0^{(1,2)}]^2 = -a_{1,2}\epsilon \tag{40}$$

for the FP (37),

$$[\gamma_+^{(1)}]^2 = 2a_1\epsilon, [\gamma_+^{(2)}]^2 = -a_2\epsilon \tag{41}$$

for the FPs (38), and

$$[\gamma_-^{(1)}]^2 = -a_1\epsilon, [\gamma_-^{(2)}]^2 = 2a_2\epsilon \tag{42}$$

for the FPs (39). Obviously, the FP (37) is stable at $\epsilon>0$ (which means $q>q_U$), and unstable at $\epsilon<0$ ($q<q_U$). The FP (38) is unstable (through the eigenvalue $\gamma_+^{(1)}$), and the FP (39) is unstable too (through the eigenvalue $\gamma_-^{(1)}$).

These properties mimic all the basic stability features reported above, *viz.*, the instability of the $UVW$ soliton close to the bifurcation point and the fact that the $U$ soliton is unstable at $q<q_U$ and stable in the region $q>q_U$. The other above-mentioned fact, that the stability margin of the $U$ soliton in the region $q>q_U$ is small (at small $\epsilon$), is also accounted for by the normal-form system, as the unstable FP (38) is quite close to the stable one (37) at small positive $\epsilon$, hence weak finite perturbations, with an amplitude comparable to the separation between the coexisting stable and unstable FP, may destabilize the former one.

The normal form expected to describe the bifurcation at the point $q=q_W$ is simpler, as it is enough to conjecture a single equation for a variable $\xi(z)$:

$$\frac{d^2\xi}{dz^2} = \xi(\epsilon - \xi^2), \tag{43}$$

where, this time, $\epsilon \equiv (q-q_W)/|q_W|$, and it is conjectured that $\xi$ is a linear combination of the amplitudes $U(x=0)$ and

$V(x=0)$. Actually, in this case we are dealing with a standard pitchfork bifurcation [24].

Equation (43) has the fixed points

$$\xi^{(0)} = 0, \tag{44}$$

which corresponds to the $W$ soliton, and

$$\xi^{(+)} = \pm\sqrt{\epsilon}, \text{for } \epsilon > 0, \tag{45}$$

which corresponds to the $UVW$ soliton. The stability eigenvalues of the FP (44) are given by $\gamma_0^2=\epsilon$, which immediately means that the $W$ soliton is stable at $q<q_W$ (i.e., $\epsilon<0$), and unstable at $q>q_W$ (i.e., $\epsilon>0$). The stability eigenvalues for the FP (45) are given by $\gamma_-^2=-2\epsilon$, which means that the $UVW$ soliton is stable where it exists (at $\epsilon>0$, i.e., $q>q_W$). These features closely resemble those reported above on the basis of direct simulations.

### E. Three-wave solitons in the case of self-defocusing $\chi^{(3)}$ nonlinearity

The stability of the same soliton family was also tested for the case of the self-defocusing $\chi^{(3)}$ nonlinearity, i.e., for $\gamma<0$. In this case, the $UVW$ solitons were found to be strongly unstable in all the cases. A typical example is shown in Fig. 10 for $k=2, q=1, \gamma=-0.02$, and $\epsilon=0$. The solution keeps the original shape for a while, but then it seems to blow up into a state of spatiotemporal turbulence (the blow-up never generates a breather, in this case). The turbulent state contains many small-scale large-amplitude spikes, therefore it is rather difficult to accurately analyze its dynamical and statistical properties. Very accurate investigation of this regime could require to use a numerical scheme with a special adaptive mesh, which is not an objective of the present work. However, we took care to check that the blow-up is not a numerical artifact. To this end, the simulations were rerun several times, consecutively decreasing the stepsize in both the $x$ and $z$ directions. In particular the picture shown in Fig. 10 was reproduced taking the former stepsize as $\Delta x=1/48, 1/96$, and $1/256$ (in the present notation), while the latter stepsize was chosen as $\Delta z=(\pi/40)\Delta x$. In all the cases tested this way, using the finer mesh never produced any visible change in the result. Therefore, we believe that the blow-up is a real effect, although its further detailed study is necessary.
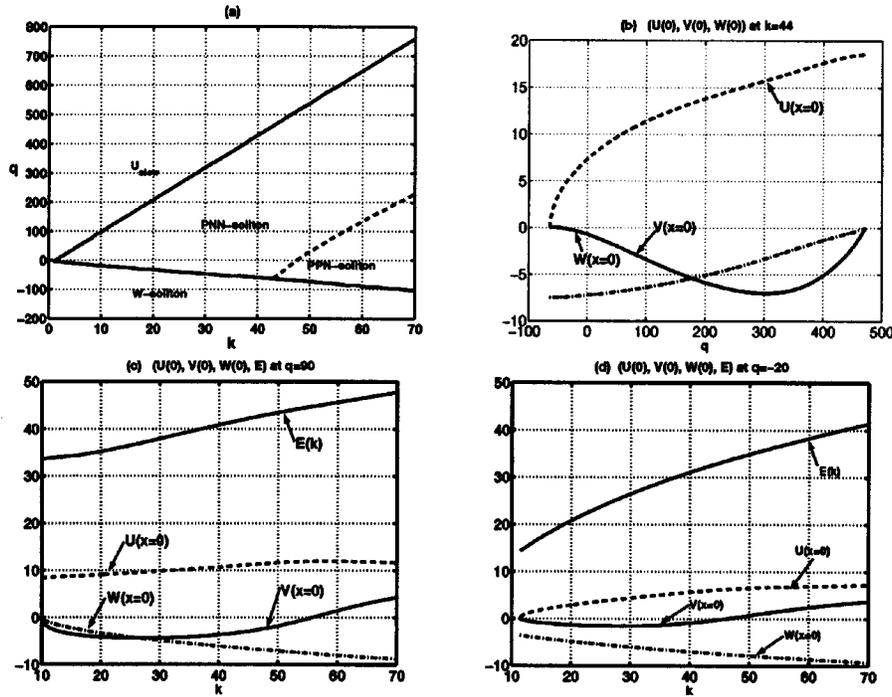
FIG. 11. (a) The existence region of the *PNN* and *PPN* solitons. (b) The amplitudes $U(x=0), V(x=0), W(x=0)$ vs $q$ for $k=44$. (c) and (d) $U(x=0), V(x=0), W(x=0)$, together with the power $E(k)$, are displayed vs $k$ for $q=90$ and $q=-20$, respectively.

It should also be mentioned that, in the limit of $\gamma \to -0$, the 3W soliton goes over into its counterpart in the vectorial model with the pure $\chi^{(2)}$ interaction, where, generally, such solitons are stable [20]. We did not try to follow this transition at extremely small negative values of $\gamma$, as the issue is a rather formal one.

### F. Three-wave solitons with different signs of the components

Similar to what was done before, we also tested stability of solitons which have different signs of their different components, cf. Eq. (31). In this case, we again focus on the case of $\gamma=1$. In particular,, starting from the exact solution (31) for $b=\gamma=0$ with $V=W=-U$ (which is the *PNN* type, according to the nomenclature introduced above), continuing the solution numerically to $b=\gamma=1$, and then varying $k$ and $q$, we were able to find a soliton branch which keeps $W(x)$ negative. The field $V(x)$ is negative at first, and then it becomes positive when $k$ becomes sufficiently large. Accordingly, the solitons change their type from *PNN* to *PPN*. This branch corresponds to branch 1 of the variational solutions in Fig. 2.

The existence region of the *PNN* and *PPN* solitons is plotted in Fig. 11(a), the dashed line indicating where the change between *PNN* and *PPN* occurs. The region is bounded by the $U$ solitons (18) from above, and the $W$ solitons (20) from below. The amplitudes $U(x=0), V(x=0), W(x=0)$ are plotted against $q$ for $k=44$ in Fig. 11(b) (this is the largest $k$ for which the $V$ component never crosses zero as $q$ increases). For $k>44$, the branch starts out as a *PPN* soliton for small $q$, and then carries over into a *PNN* one as $q$ increases. The set of the amplitudes $[U(x=0), V(x=0)$

$=0), W(x=0)]$ is also plotted in Fig. 11(b)–11(d) against $k$ for $q=90$ and $q=-20$, along with the corresponding power function $E(k)$ defined in Eq. (5). As it was mentioned already, there is a point where $V(x=0)$ changes its sign. We stress that, at this point, the soliton's $V$ component as a whole is *not* zero. Instead, close to the point, the solution changes its shape from the normal single-hump one to a multihumped shape, however with a relatively small amplitude.

Since the VK condition (14) is satisfied everywhere for these newly introduced 3W soliton solutions [see Figs. 11(c) and 11(d)], it remains to test the stability of the solutions in direct simulations. The result for $k=5$ is shown in the second plot of Fig. 6. As $q$ increases, the stable $W$ soliton bifurcates to an unstable *PNN*-soliton. As $q$ continues to increase, the latter one becomes stable. Eventually, it becomes unstable again. Finally, as $|v|$ and $|w|$ decrease, the *PNN* soliton degenerates into a stable $U$ soliton.

We now describe in detail a stability test of the *PNN*-type soliton for $(k,q)=(6.4,4)$, which turns out to be a delicate case. With a perturbation amplitude of $\epsilon=0.02$, the soliton develops into a breather, with noticeable energy shedding in the $u$ and $v$ components, as shown in Fig. 12. However, when the perturbation was slashed to $\epsilon=0.01$, a similar breather, with almost the same amplitude, did develop, but not until having passed essentially twice the distance of the $\epsilon=0.02$ case (for $\epsilon=0.01$, the amplitude of the $v$ component first peaked at $z \approx 10.8$, whereas for $\epsilon=0.02$, this first happened at $z \approx 5.2$.) Reducing the perturbation further to $\epsilon=0.005$ reveals that the *PNN* soliton is now actually *stable*, remaining close to the unperturbed one, at least for $z$ up to 120. What this most plausibly means is that the *PNN* soliton is stable indeed, but with a very narrow stability basin, and
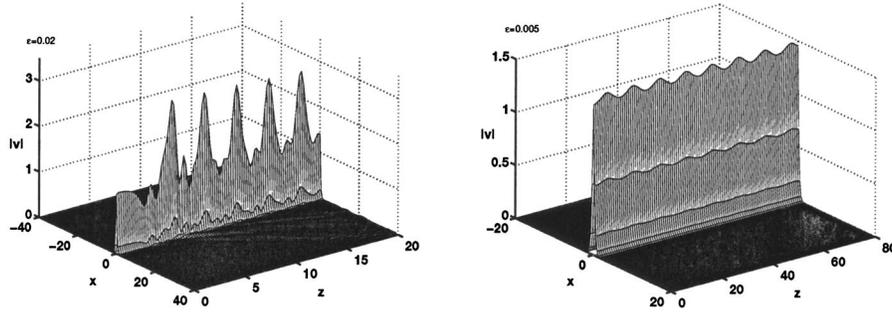
FIG. 12. Evolution of a stable soliton of the *PNN* type, at $k=6.4$ and $q=4$, under the action of the initial perturbations [see Eq. (33)] with $\epsilon=0.02$ and $\epsilon=0.005$.

with breather states located nearby (a similar situation was encountered above in the *PPP* case).

The stability of the *PPN* solitons was tested too, and they were found to be unstable. For example, in the case of $(k,q)=(60,20)$, the soliton of this type always evolves into a breather, even as $\epsilon$ approaches zero (in this case, very small stepsizes in $x$ and $z$ have to be used in the simulations, because of the large value of $k$); actually, the *PPN* soliton manifests its instability even in the simulations with $\epsilon=0$. The instability of the *PPN* solitons is not surprising, since the $\chi^{(2)}$ term (25) in the system's Hamiltonian is positive for them (unlike the *PNN* soliton, for which it is negative).

Two other branches of solitons were also found. One is in some sense the reverse of the *PNN*—it is the *PPN* branch shown in Fig. 11. It carries solitons of the *PPN* type at $k$ small; as $k$ increases, the $u$ amplitude changes its sign, and the soliton switches into the *NPN* type (which is actually tantamount to the *PNN* type, due to the symmetry against the simultaneous change of the signs of $U$ and $V$). Another branch carries solitons of the *PNP* type. These two branches provide for a crossover between the $W$ and $V$ solitons. We do not aim here to describe them in detail; however, we mention that the solitons of the *NPN* type make the term (25) negative, and, as it might be expected, they are stable in some cases. On the contrary, all the solitons of the *PNP* and *PPN* types are unstable, evolving into stable breathers. Their instability is simply explained by the fact that, as well as for their *PPN* counterparts, the $\chi^{(2)}$ interaction term (25) in the Hamiltonian is positive for them.

### G. Soliton solutions in the case of zero birefringence

As stated before, the birefringence parameter $b$ in the underlying Eqs. (1)–(3) could be rescaled to 1, unless $b=0$. In the latter case, solitons exist and have $U=\pm V$. Typical examples of these solitons were also tested for the stability. As one may anticipate on the basis of the above results, the stability of any soliton is basically determined by the sign which it lends the $\chi^{(2)}$ Hamiltonian term (25). For instance, we have found that the *PPP* and *PNN* solitons with $b=0$ and $(k,q)=(2,1)$ are stable. On the other hand, the *PPN* and *PNP* solitons with $b=0$ were found to be unstable, evolving into stable breathers in direct simulations.

### VI. CONCLUSION

In this paper, we have introduced a general model of three-wave interactions in the spatial domain for an optical

waveguide, which combines $\chi^{(2)}$ and $\chi^{(3)}$ nonlinearities, the latter including SPM, XPM, and FWM terms. Both self-focusing and self-defocusing $\chi^{(3)}$ nonlinearities were considered. The birefringence of the two fundamental waves, and the phase mismatch between them and the second harmonic were taken into regard. The model can be realized experimentally by means of the QPM technique in quadratically nonlinear birefringent media. Several types of solitons were found by means of the variational approximation and numerical methods: single-component ones (for which exact solutions are available) and generic 3W solitons of different types, classified by relative signs of the their components. The 3W solitons were constructed by means of the variational approximation, and in a numerical form. In some parametric regions, the solitons overlap with the continuous spectrum and are therefore delocalized (or might even be of the embedded type).

These solitons are amenable to experimental observation in essentially the same range of physical parameters where two-wave solitons were already predicted in models with the competing $\chi^{(2)}$ and $\chi^{(3)}$ nonlinearities, Refs. [1] and [2]. In fact, the use of the birefringence, which often helps to match the fundamental and second harmonics, can make the creation of solitons in such a system more feasible than in the usual two-wave settings employing the QPM technique.

Stability of the solitons was tested in direct simulations, and it was concluded that it, generally, complies with two theoretical predictions: First, soliton families tend to be stable if the VK criterion is satisfied for them; second, the cubic term (25) in the Hamiltonian density, which accounts for the $\chi^{(2)}$ coupling between the three waves, must be negative for the stability. As a result, it was concluded that the 3W soliton family of the *PPP* type (with positive fields in all the components) is mostly stable. The *PNN* family is stable, but only in the marginal sense. It was also found that the fast single-component fundamental-frequency soliton is unstable in most cases, but, nevertheless, it features a narrow stability interval. Its slow counterpart and the single-component second-harmonic soliton may be both stable and unstable. The possibility that the fast single-component soliton and the second-harmonic one may be stable in some cases are unexpected results, which we not reported in other models.

Unstable solitons do not decay into radiation, but rather evolve into stable breathers. A different instability was found in the case of the self-defocusing $\chi^{(3)}$ nonlinearity: in this case, the solitons blow up into a turbulent state with a large number of narrow spikes.

Parallel to the consideration of the solitons, CW solutions were also studied, with a conclusion that their existence and stability (against CW perturbations) generally correlate with those of analogous solitons.

## ACKNOWLEDGMENTS

[1] C. Etrich, F. Lederer, B. A. Malomed, T. Peschel, and U. Peschel, Prog. Opt. **41**, 483 (2000).

[2] A. V. Buryak, P. Di Trapani, D. V. Skryabin, and S. Trillo, Phys. Rep. **370**, 63 (2002).

[3] W. E. Torruellas, Z. Wang, D. J. Hagan, E. W. VanStryland, G. I. Stegeman, L. Torner, and C. R. Menyuk, Phys. Rev. Lett. **74**, 5036 (1995).

[4] A. Kaplan and B. A. Malomed, Opt. Commun. **211**, 323 (2002).

[5] S. Carrasco, H. Kim, G. Stegeman, P. Loza- Alvarez, and L. Torner, Opt. Lett. **27**, 2016 (2002).

[6] C. B. Clausen, O. Bang, and Y. S. Kivshar, Phys. Rev. Lett. **78**, 4749 (1997).

[7] J. F. Corney and Ole Bang, Phys. Rev. E **64**, 047601 (2001).

[8] O. Bang and J. F. Corney, Opt. Photonics News **12**, 42 (2001).

[9] O. Bang, C. B. Clausen, P. L. Christiansen, and L. Torner, Opt. Lett. **24**, 1413 (1999); S. K. Johansen, S. Carrasco, L. Torner, and O. Bang, Opt. Commun. **203**, 393 (2002).

[10] P. Di Trapani, A. Bramati, S. Minardi, W. Chinaglia, C. Conti, S. Trillo, J. Kilius, and G. Valiulis, Phys. Rev. Lett. **87**, 183902 (2001).

[11] G. P. Agrawal, *Nonlinear Fiber Optics* (Academic Press, San Diego, 1995).

[12] K. J. Blow, N. J. Doran, and D. Wood, Opt. Lett. **12**, 202 (1987).

[13] S. H. Zhu, G. X. Huang, and W. N. Cui, Chin. Phys. **11**, 919 (2002).

[14] B. A. Malomed, Prog. Opt. **43**, 71 (2002).

[15] M. G. Vakhitov and A. A. Kolokolov, Radiophys. Quantum Electron. **16**, 783 (1973).

[16] L. Bergé, Phys. Rep. **303**, 259 (1998).

[17] D. J. Kaup, T. I. Lakoba, and B. A. Malomed, J. Opt. Soc. Am. B **14**, 1199 (1997).

[18] A. R. Champneys, B. A. Malomed, J. Yang, and D. J. Kaup, Physica D **152-153**, 340 (2001); J. Yang, B. A. Malomed, D. J. Kaup, and A. R. Champneys, Math. Comput. Simul. **56**, 585 (2001).

[19] P. Di Trapani, D. Caironi, G. Valiulis, A. Dubietis, R. Danielus, and A. Piskarskas, Phys. Rev. Lett. **81**, 570 (1998).

[20] U. Peschel, C. Etrich, F. Lederer, and B. A. Malomed, Phys. Rev. E **55**, 7704 (1997).

[21] D. J. Kaup and B. A. Malomed, Physica D **184**, 153 (2003).

[22] W. L. Kath and N. F. Smyth, Phys. Rev. E **51**, 1484 (1995).

[23] See L. F. Shampine, M. W. Reichelt, and J. Kierzenka, ftp://ftp.mathworks.com/pub/doc/papers/bvp/

[24] G. Iooss and D. D. Joseph, *Elementary Stability and Bifurcation Theory* (Springer-Verlag, New York, 1980).